

Using integrated data analysis to extend measurement capability (invited)

L. M. Reusch, M. D. Nornberg, J. A. Goetz, and D. J. Den Hartog

Citation: [Review of Scientific Instruments](#) **89**, 10K103 (2018); doi: 10.1063/1.5039349

View online: <https://doi.org/10.1063/1.5039349>

View Table of Contents: <http://aip.scitation.org/toc/rsi/89/10>

Published by the [American Institute of Physics](#)

Articles you may be interested in

[Active spectroscopy measurements of the deuterium temperature, rotation, and density from the core to scrape off layer on the DIII-D tokamak \(invited\)](#)

[Review of Scientific Instruments](#) **89**, 10D110 (2018); 10.1063/1.5038349

[Incorporating magnetic equilibrium information in Gaussian process tomography for soft X-ray spectroscopy at WEST](#)

[Review of Scientific Instruments](#) **89**, 10F103 (2018); 10.1063/1.5039152

[Helium line ratio spectroscopy for high spatiotemporal resolution plasma edge profile measurements at ASDEX Upgrade \(invited\)](#)

[Review of Scientific Instruments](#) **89**, 10D102 (2018); 10.1063/1.5034446

[Conceptual design of extended magnetic probe set to improve 3D field detection in NSTX-U](#)

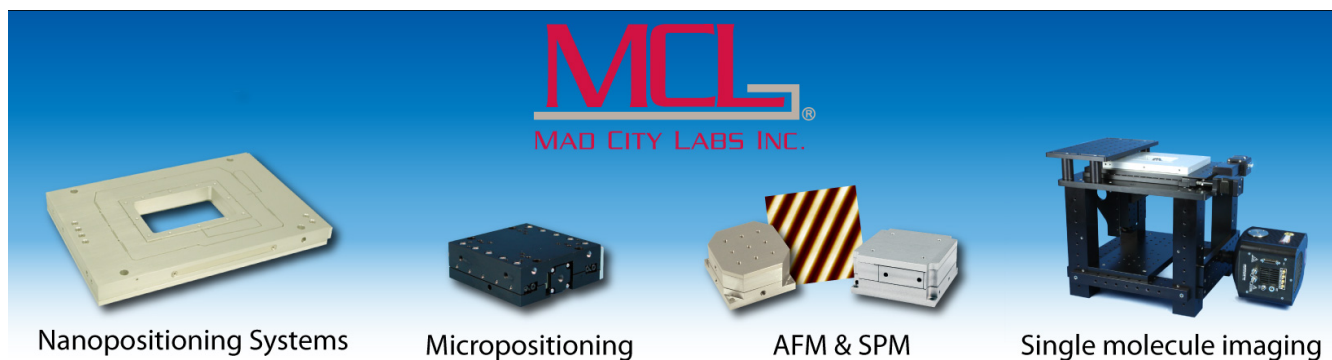
[Review of Scientific Instruments](#) **89**, 10J108 (2018); 10.1063/1.5036942

[Synthetic diagnostic for assessing spatial averaging of charge exchange recombination spectroscopy measurements](#)

[Review of Scientific Instruments](#) **89**, 10D101 (2018); 10.1063/1.5036964

[Sub-millisecond electron density profile measurement at the JET tokamak with the fast lithium beam emission spectroscopy system](#)

[Review of Scientific Instruments](#) **89**, 043509 (2018); 10.1063/1.4986621



MCL
MAD CITY LABS INC.

Nanopositioning Systems Micropositioning AFM & SPM Single molecule imaging

Using integrated data analysis to extend measurement capability (invited)

L. M. Reusch,^{a)} M. D. Nornberg, J. A. Goetz, and D. J. Den Hartog
 University of Wisconsin-Madison, Madison, Wisconsin 53706, USA

(Presented 19 April 2018; received 7 May 2018; accepted 12 July 2018;
 published online 10 August 2018)

The analysis approach called integrated data analysis (IDA) provides a means to exploit all information present in multiple streams of raw data to produce the best inference of a plasma parameter. This contrasts with the typical approach in which information (data) from a single diagnostic is used to measure a given parameter, e.g., visible bremsstrahlung $\rightarrow Z_{\text{eff}}$. Data from a given diagnostic usually contain information on many parameters. For example, a Thomson scattering diagnostic is sensitive to bremsstrahlung and line emission in addition to electron temperature. This background light is typically subtracted off and discarded but could be used to improve knowledge of Z_{eff} . IDA encourages explicit awareness of such information and provides the quantitative framework to exploit it. This gives IDA the ability to increase spatial and temporal resolution, increase precision and accuracy of inferences, and measure plasma parameters that are difficult or impossible to measure using single diagnostic techniques. One example is the measurement of Z_{eff} on Madison symmetric torus using IDA since no single diagnostic can provide a robust measurement. As we enter the burning plasma era, application of IDA will be critical to the measurement of certain parameters, as diagnostic access in the harsh fusion environment will be extremely limited. *Published by AIP Publishing.*
<https://doi.org/10.1063/1.5039349>

I. INTRODUCTION

Individual plasma diagnostics are often considered to be a means for obtaining a direct measurement of a particular physical plasma parameter, e.g., visible bremsstrahlung monitor \rightarrow the effective ion charge (Z_{eff}) of a plasma, Thomson scattering \rightarrow electron temperature (T_e) and density, or interferometer \rightarrow electron density (n_e). Little conceptual distinction is made between a parameter itself and the measurement of that parameter using a specific diagnostic, almost as if a direct translation could be made between the diagnostic raw data and the physical parameter of interest. In reality, the raw data from a diagnostic only provide part of the measurement of a particular plasma parameter. There is always an analysis or inference step that is an integral part of the measurement of that parameter. The inference step provides the means to extract an estimate of the plasma parameter of interest from the raw diagnostic data; however, diagnostic data also often contain information pertaining to a variety of other physical parameters, and this “hidden” information is usually ignored or removed during the inference step. Explicit awareness of such information presents the possibility of providing information on all parameters.

A simple example is the background light subtraction usually implemented for the analysis of Thomson scattering (TS) raw data. The background light contains substantial emission from bremsstrahlung and line radiation and could be used to improve the measurement of Z_{eff} (and other parameters). However, the background in the raw TS signal is often fit to some

curve and the information is discarded. The only information retained during the inference is that associated with the laser pulse itself.

Another example of this is the two-color (or multi-color) technique to infer T_e using soft X-ray (SXR) brightness signals. The emitted SXR spectrum of a plasma contains a wealth of information about the plasma. In particular, SXR measurements are sensitive to T_e , n_e , and impurity densities. There are a number of atomic processes that are important for a given set of values for these parameters that give rise to a combination of bremsstrahlung, radiative and dielectronic recombination, and line radiation. The continuum spectrum (consisting of bremsstrahlung and recombination emission), in particular, follows the form¹

$$\varepsilon \propto \sum_x \frac{n_e n_x Z_x^2}{\sqrt{T_e}} e^{-E/T_e} \times [g_{ff} + recomb.], \quad (1)$$

where ε is the spectral emissivity, n_x and Z_x are the density and charge of a given ion charge state x (including impurity and majority species), E is the energy of the emitted X-ray photon, and the sum is taken over all charge states of all ion species. Note, in particular, that the slope of the continuum depends only on T_e , so the measurement of the slope enables the measurement of T_e .

In the two color technique, the measurement of the slope is accomplished by taking the ratio from different SXR brightness detectors that share the same line of sight but are equipped with different thickness filters to sample different regions of the SXR spectrum.^{2,3} Taking this ratio removes dependence on n_e and ion content (n_x , Z_x), enhancing the sensitivity to T_e ; however, this method also discards a significant amount of information about the plasma. As will be discussed more fully later, explicit acknowledgment and subsequent use of

Note: Paper published as part of the Proceedings of the 22nd Topical Conference on High-Temperature Plasma Diagnostics, San Diego, California, April 2018.

^{a)}lmmcguire@wisc.edu

this information allows extra knowledge about the plasma to be extracted.

Integrated data analysis (IDA) encourages awareness of such hidden or ignored information, and, importantly, provides a framework with which to exploit it. Additionally, there is often information available from modeling or other sources of background information. The framework of IDA also allows for explicit inclusion of such information. The goal of IDA is to use all the information present both within the data from various complementary diagnostics and from other sources (e.g., modeling) in order to obtain the most accurate and reliable parameter measurements in a transparent and standardized way. This synergistic combination of information often produces a result that extracts additional scientific values from each individual measurement given by a set of diagnostics.

This paper introduces IDA and the Bayesian framework used, highlights the possibilities for expanded measurement capabilities by using all the information available in the raw data, and illustrates how such information can be used. Section I introduces the Bayesian analysis which forms the framework that is often used for IDA and illustrates how IDA is accomplished, Sec. II discusses the benefits of IDA using a Bayesian framework and how it can result in increased measurement capabilities, and Sec. III provides an example of the implementation of IDA to measure Z_{eff} in the Madison Symmetric Torus (MST) with particular focus on how we have taken advantage of the information that is available in the diagnostics used.

II. INTRODUCTION TO BAYESIAN ANALYSIS

A natural framework in which to implement IDA is Bayesian analysis. Bayesian analysis itself can be applied to a broad set of inference problems and is widely used in the community to infer plasma parameters from single diagnostics (see Refs. 4–8 for some examples). While several sources do a much more thorough treatment of Bayesian analysis,^{9,10} a brief introduction is presented here. The core of Bayesian analysis is Bayes' rule,⁹

$$p(\theta|x, I) = \frac{\mathcal{L}(x|\theta, I)\pi(\theta|I)}{p(x|I)}, \quad (2)$$

where θ represents the model parameters, typically the plasma parameters of interest, and can be an array of multiple parameters. The diagnostic data is x , and I is any background information available. Here, $p(\theta|x, I)$ is called the posterior distribution function, $\mathcal{L}(x|\theta, I)$ is the likelihood function, and $\pi(\theta|I)$ is the prior distribution. Finally, $p(x|I)$ is called the evidence.

The posterior distribution $p(\theta|x, I)$ is the probability of getting a particular value for parameter(s) θ , given the data x and any additional information I . This is the desired result. While the full probability distribution is the most complete answer, the result can often be approximated or interpreted as the location of the maximum in posterior distribution being the best estimate for θ , and the width of posterior distribution is the uncertainty in that estimate.

The likelihood function $\mathcal{L}(x|\theta, I)$ describes the probability of getting the data given a particular value for θ . It relates

the experimental data to the parameters of interest through a forward model. While each diagnostic has a unique forward model quantifying its details and systematics, each forward model is also characterized using the plasma parameter or parameters of interest for the inference, e.g., T_e , n_e , magnetic flux, current density, etc. In this way, the most probable value (i.e., inference) for all the parameters of interest can be found using information from all diagnostics.

The diagnostic forward model incorporates the physics of the measurement processes as well as any instrumentation effects such as calibration factors, filter transmission, etc. It also incorporates statistical sources of uncertainty such as counting noise as well as known systematic uncertainties such as uncertainty in calibration factors.

The likelihood function can incorporate background information into the analysis through the choice of forward model. The appropriateness of the model can be tested by comparing results from different models quantitatively. In fact, development of a forward model enables the explicit codification of the assumptions that necessarily go into the analysis of experimental data. Explicitly identifying and quantifying assumptions means that their effect, importance, and validity can be tested as a straightforward part of the IDA process.

Typically, θ contains only parameters of interest, however, sometimes systematic parameters are a necessary part of the forward model. These parameters are of no physical interest, making them nuisance parameters. Nuisance parameters may be eliminated from the results through “marginalization,” which simply integrates the posterior distribution over all possible values of the nuisance parameter,⁹

$$p(\theta|x, I) = \int p(\theta, \alpha|x, I)d\alpha, \quad (3)$$

where α is the nuisance parameter, and the integral is taken over all possible values for α . The result is the probability of getting a particular set of values for θ , regardless of the exact value of α . This procedure can also be used to create 2-dimensional projections of multi-parameter distributions in order to identify correlations between specific parameters.

The prior distribution $\pi(\theta|I)$ represents background knowledge. This can be as simple as the range in which the results are expected to fall, and often these ranges can be informed by physical constraints (e.g., T_e must be positive or Z_{eff} must be at least 1). Prior probabilities can also contain more nuanced information, again allowing extra knowledge about the system to be included quantitatively. As with likelihood functions, explicit identification and quantification of the assumptions specifically related to the parameters of interest can be encoded in the prior. This allows their effect, importance, and validity to be tested.

The normalization factor in the denominator $p(x|I)$ is called the evidence and is used to calculate the absolute probability of $p(\theta|x, I)$. Many situations involve parameter estimation, and as such, the relevant information is the location of the maximum in the posterior distribution, not the absolute magnitude of the probability, so the evidence can safely be ignored. However, there are certain times when calculation of this evidence is very important. Such situations include

choosing between two or more descriptions of the underlying phenomenon (i.e., model discrimination), identifying and possibly resolving diagnostic inconsistencies, or during diagnostic design when identifying which measurements will add the most information to the inference of θ .

An illustration of how IDA is accomplished using this Bayesian framework is shown in Fig. 1 for T_e and carbon density n_C (i.e., $\theta = \{T_e, n_C\}$) for two different potential combinations of diagnostics. The top row in Fig. 1 shows likelihood functions for synthetic data as a function of T_e and carbon density for absolute SXR brightness in (a) and charge exchange recombination spectroscopy (CHERS) in (b) for the same location in the plasma. The resulting posterior distribution obtained after multiplying these likelihoods together is shown in (c). In the bottom row, a second illustration of the same parameters is shown, this time using SXR brightness (d) and TS (e). The resulting posterior is shown in (f). For these illustrations, the prior probability distributions were uniform probabilities over the range of the plots (i.e., $900 \leq T_e \leq 1900$ eV).

The illustrations of IDA in Fig. 1 show that the process of IDA is largely the same regardless of diagnostics. The illustrations also show how the combination of complementary diagnostics can potentially provide constraints on seemingly dissimilar parameters. Here, the likelihood function for the synthetic SXR brightness signal is based on modeled absolute brightness, assuming that carbon is the only impurity in the plasma. Recall from Eq. (1) that absolute SXR signals are sensitive to both impurity density and T_e . The CHERS signal contains no explicit information on T_e . Nevertheless,

the combination of CHERS data with the SXR data helps to constrain T_e . The second row in Fig. 1 illustrates a similar effect when combining TS and SXR. Even though the TS data is not sensitive to carbon density, the combination is a more precise inference of both the carbon density and T_e .

III. BENEFITS OF IDA

Integrated data analysis is a subset of Bayesian analysis applications that specifically makes use of multiple diagnostics. As a concept, IDA has a well-developed and robust intellectual foundation¹⁰⁻¹³ and is distinct from Bayesian analysis of single diagnostics. In particular, there are concrete benefits from combining multiple complementary diagnostics that allows for the extraction of the maximum amount of scientific knowledge from a given set of diagnostics. These benefits can improve or extend measurement capability and include the following:

- Improved measurement precision and resolution.
- Straightforward inclusion of uncertainties from both statistical and systematic sources.
- Simplified uncertainty analysis particularly when uncertainties are non-Gaussian and/or correlated
- Inclusion of both qualitative and quantitative background information.
- Improved measurement accuracy:
 - Validation of data and/or models.
 - Identification of diagnostic inconsistencies.
 - Estimation of systematic uncertainties or errors.

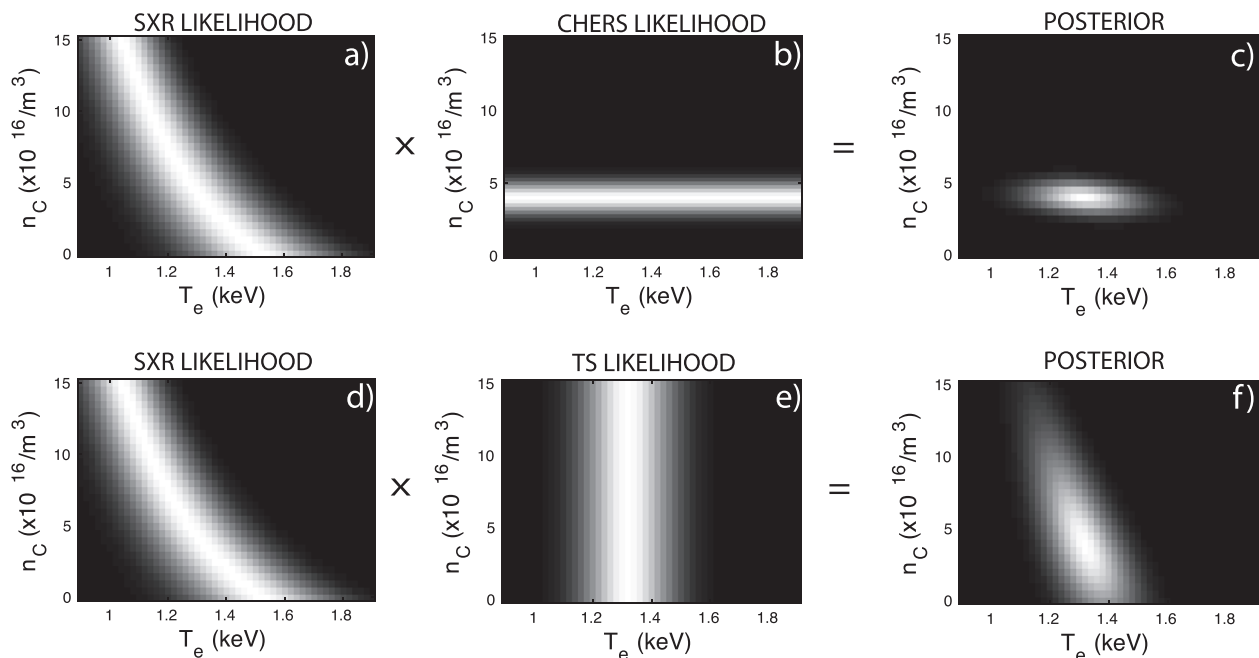


FIG. 1. Illustration of using a Bayesian framework to accomplish IDA. Likelihood functions using synthetic data are shown for a single measurement location looking at the core of the plasma. Here, lighter shading represents higher probability and darker shading represents lower probability. In the top row, (a) shows the likelihood function for a SXR brightness measurement, (b) shows the likelihood function for a CHERS signal, and (c) shows the resulting posterior probability. In the second row, a second illustration with a different combination of diagnostics is shown, again using synthetic data. The same SXR brightness likelihood function is shown in (d), a likelihood function for a TS point is shown in (e), and the resulting posterior is shown in (f). This figure follows the form of a presentation by Fischer in Ref. 11.

- Determination of parameters for which an estimate is difficult to obtain using any single diagnostic.

The following examples illustrate some of these benefits and show how application of IDA results in better measurements needed to address the needs of their respective scientific programs. All of these examples used a Bayesian framework for IDA.

Again, at the most basic level, IDA enables improved measurement precision and resolution simply by identifying and combining relevant data from multiple diagnostics. An example is from the work pursued at the TJ-II stellarator where IDA was developed to infer the density profile evolution using information from interferometry, reflectometry, and TS. Here, the TS diagnostic provided density profile shape information with high precision, but, since it was single pulse, it had no ability to inform profile evolution. On the other hand, the reflectometry and interferometry diagnostics could provide density information on a times scale of ~ 1 ms, but the inferred profiles were too uncertain to study the profile evolution without additional shape information. IDA provided the framework that allowed a self-consistent combination of information from three diagnostics: interferometry provided information on the absolute density in the core, TS provided information on the shape of the central density profile, and reflectometry provided the edge density profile at high time resolution. The resulting density profiles had both the time resolution and precision necessary to study edge profile evolution¹⁴ and enabled studies of L-H transitions and the dynamics involved in the formation of other transport barriers.¹⁵

The IDA framework also makes it possible to increase measurement accuracy. By enforcing consistency between diagnostics, and incorporating all known systematic effects, it is possible to quantitatively identify diagnostic inconsistencies. This in turn means that it is possible to identify and sometimes estimate previously unknown systematic effects, errors in calibrations, or problems in the interpretation method. In many cases, the process of identifying inconsistencies can suggest specific improvements to be done, which will ideally resolve such inconsistencies.

An example of this comes from the ASDEX-Upgrade tokamak where IDA helped determine that uncertainties in the location of flux surfaces led to errors in the reconstruction of n_e profiles. IDA is routinely applied at ASDEX-Upgrade to reconstruct T_e and n_e profiles using information from lithium beam excitation spectroscopy, interferometry, electron cyclotron emission (ECE), and TS.¹⁶ Here, IDA was employed to rigorously and systematically evaluate data quality from each individual diagnostic, taking into account all known systematic and statistical errors. This systematic examination of the diagnostic data identified inconsistencies between reconstructions of n_e profiles when incorporating data from TS compared to using just data from the Li-beam, interferometry, and ECE. This inconsistency ultimately was due to the uncertainty in the underlying equilibrium reconstruction, in particular uncertainty in the location of the flux surfaces, and that incorporating the data from TS produces more accurate n_e profiles. While the correction was relatively small, and localized to the pedestal, it was quite important in enabling

accurate studies of pedestal physics being pursued at ASDEX-Upgrade.¹⁷⁻¹⁹ In addition, the T_e and n_e profiles are now used as constraints on the equilibrium reconstructions.²⁰ This example illustrates how the integration of diagnostics that have different systematic effects (e.g., TS is a local measurement, but interferometry is line-integrated) helped to identify some unknown systematic uncertainties, the understanding of which lead to higher accuracy in the resulting profile.

The Joint European Torus (JET) tokamak and the Wendelstein 7-X stellarator are pursuing equilibrium and other plasma profile reconstructions using the many diagnostics embedded in the Minerva framework²¹ in order to incorporate non-Gaussian uncertainties and simplify error analysis. In fact, most equilibrium reconstruction algorithms combine information from multiple diagnostics. However, many use global least squares or other minimization techniques to reconstruct profiles of interest, making the addition of new diagnostics difficult. Furthermore, if error estimates are provided at all, they are usually calculated by following statistical uncertainty propagation rules, which may neglect important correlations, or sometimes by a Monte Carlo error analysis, making the impact of additional diagnostics difficult to determine.

Integrated data analysis using Bayesian analysis is a natural framework in which to do equilibrium reconstructions because the use of likelihood functions makes the analysis highly modular. Addition of new diagnostics can be implemented as the diagnostic becomes available. Because IDA provides a rigorous way to encode both the statistical and systematic uncertainties for each diagnostic, error analysis can potentially be simplified and streamlined. This is true particularly when uncertainties are non-Gaussian, correlated, and/or otherwise ill-behaved (e.g., the probability distribution is multi-modal).

Finally, IDA enables determination of parameters for which an estimate is difficult to obtain using any single diagnostic. One good example of this is the measurement of Z_{eff} . Many measurements contain some information about Z_{eff} ; however, it is often not the dominant effect, or diagnostic signals are contaminated with unknown systematic effects, making it difficult to extract the value of Z_{eff} using a single diagnostic, but the combination of information from multiple diagnostics can make the Z_{eff} measurement feasible. An illustration of this (to be discussed in Sec. IV) comes from the development of an IDA approach at the MST reversed field pinch to measure Z_{eff} profiles.

IV. IDA MEASUREMENT OF Z_{EFF} ON MST

Over the years, significant effort has been applied to determine Z_{eff} in MST; however, no single diagnostic currently available on MST has been able to provide an unambiguously accurate measurement of Z_{eff} . Visible and near-infrared bremsstrahlung measurements were contaminated with molecular line emission and electron-neutral bremsstrahlung radiation.²² Analysis of X-ray spectroscopy measurements was compromised by a lack of knowledge about, and an inability to estimate, the spectral contribution from continuum recombination radiation.²³ These single diagnostic attempts suffered

from systematic effects that were impossible to account for. IDA overcomes these difficulties by combining data from multiple diagnostics, allowing the extraction of a reliable Z_{eff} profile on MST.

The IDA approach developed at MST measures T_e and n_Z (thus by extension Z_{eff}) profiles by coupling data from the TS diagnostic and the absolutely calibrated SXR tomography system. This approach takes advantage of all of the information available in absolute SXR brightness measurements as discussed earlier along with substantial information from previous impurity studies using the CHERS diagnostic.^{24–27}

Although the forward models have been described elsewhere, some time will be spent highlighting the information available that is incorporated into the analysis. The TS diagnostic is a multi-point, multi-pulse TS system measuring from the center of MST to the edge with 21 spatial points and a nominal temporal resolution of 2 kHz.²⁸ The forward model for TS predicts the number of detected photons given a local T_e and n_e assuming a relativistic Maxwellian distribution for electron energies.²⁹ Detector and spectral calibrations are taken into account; however, the diagnostic has not been absolutely calibrated for n_e , so it is treated as a nuisance parameter and marginalized out of the TS analysis.³⁰ While we are explicitly aware of the additional information in the raw TS, we do not yet take advantage of it.

The two-color soft X-ray tomography diagnostic has 40 unique and overlapping viewing chords distributed across 4 cameras at a single toroidal location. Each chord is equipped with two filtered silicon AXUV4BST photo-detectors that sample the same plasma volume.³¹ For each chord, one detector is typically equipped with a thinner beryllium filter and the other is equipped with a thicker beryllium filter. While the tomography system is typically operated in this two-color mode, the filter configuration is flexible, and, for example, 8 different thickness filters can be used for increased spectral information.³²

This diagnostic has been absolutely calibrated, which makes comparisons to models of absolute brightness feasible. This includes bench tests to determine the exact amplification factor provided by the transimpedance amplifiers for frequencies between 1 and 100 kHz; calibration of the beryllium filter transmission using the BESSY II electron storage ring for photon energies between 1.8 and 10 keV;³³ accounting of all geometric effects such as non-normal incidence of photons; and accounting for the presence of an aluminum frame on the silicon detectors, which can change the spectral response of the detector.³⁴

The forward model for the SXR diagnostic predicts absolute SXR brightness given a set of profiles for T_e , n_e , and impurity density n_Z . The n_e profile is not yet incorporated into the IDA framework, thus is specified from the experiment using interferometry and a discussion of n_Z is presented below. Temperature profiles are specified using a parameterization of the form

$$T_e(r) = T_{e0}(1 - (r/a)^\alpha)^\beta, \quad (4)$$

where T_{e0} is the core electron temperature, α and β are other free parameters that describe the shape of the profile, and a , the minor radius of the plasma, is 0.5 m. This profile

is assumed to be axisymmetric. Helical features, islands, or other features can be added to the profile if present. A full description of the geometry and the implementation of the profile can be found in Ref. 35. For the example presented here, we have assumed that the profile shape follows Eq. (4); however, we can use different profile definitions to explicitly test for the presence of non-axisymmetric features in the temperature profile.³⁶ It should be noted that while the SXT diagnostic is capable of doing tomography, no tomographic inversions were done for this analysis. Rather, a 2D cross section of the plasma emissivity is modeled using the specified profiles, and the signal for each photodetector is calculated by integrating the emissivity along the respective lines of sight.

The forward model for emissivity uses a full collisional-radiative model that predicts the relevant atomic processes that give rise to the varying amounts of bremsstrahlung, radiative and dielectronic recombination, and line radiation emitted by the plasma from the specified T_e , n_e , and n_Z . While there are many collisional radiative models available, we have been working extensively with the atomic database and analysis structure (ADAS),^{37,38} a well-developed platform for modeling radiation from astrophysical and fusion plasmas. Currently, the model uses atomic parameters based on the Cowan procedure within ADAS. A different atomic physics model may produce somewhat different results and uncertainties at the atomic level have not yet been taken into account. However, we recently used ADAS to predict SXR signals in multiple energy ranges (different filters) with differing amounts of bremsstrahlung, radiative and dielectronic recombination, and line radiation, with excellent agreement to experimental data.³² Filter, amplifier, and detector calibrations have been taken into account in the SXR forward model.

Another key piece of information necessary to model absolute SXR signals is some idea of the species and amount of impurities present in the plasma. It is impossible to properly account for the contributions from the different sources of radiation to SXR brightness measurements without some knowledge of the impurities present in the plasma. That knowledge can be provided by CHERS or other spectroscopic measurements. Such information has been provided by substantial measurements of impurity densities and dynamics in MST.^{24–27} The impurities found in these studies were typical low-Z impurities from atmospheric contamination and plasma facing components: oxygen, nitrogen, boron, and carbon. Aluminum is also present due to the close fitting Al shell that acts as the plasma first wall on MST. The studies of impurities indicate that the impurity profiles have a characteristic hollow shape to them. This was eventually determined to arise from a thermal screening effect that preferentially transports impurities toward the edge of the plasma.^{26,27} As such, the impurity profiles have been parameterized such that they are allowed to be hollow. The studies also revealed that there is a characteristic relative distribution of low-Z impurities.²⁴ We have taken advantage of such knowledge to reduce the number of free parameters included in the model. Specifically, only the aluminum and carbon density profiles are free to vary. The other low-Z impurity density profiles are scaled relative to the

carbon profile based on their characteristic relative amounts. More details on the profile parameterizations for the hollow impurity density profiles can be found in Ref. 39.

It should be noted that while information on impurities has been incorporated as prior information in the SXR forward model, no CHERS data has been incorporated due to the lack of forward model for CHERS. Development of a forward model for CHERS data is currently underway, starting with a self-consistent calculation of the neutral beam attenuation (necessary for inferring impurity density measurements from CHERS data).⁴⁰ This model uses the same impurity density profiles used in the SXR forward model and atomic cross sections to predict the neutral beam density as it traverses the plasma and is attenuated by ion collisions. The model is combined with experimental data from beam Doppler-shift spectra and shine-through particle flux to determine the local neutral beam particle density.

The IDA tool calculates the posterior probability distribution using an affine invariant Markov chain Monte Carlo technique to sample the parameter space.⁴¹ Inferences of the parameters of interest from experimental data using this IDA tool are shown in Figs. 2–5 for a single time slice. The resulting inference of the T_e profile (red curve) is shown in Fig. 2,

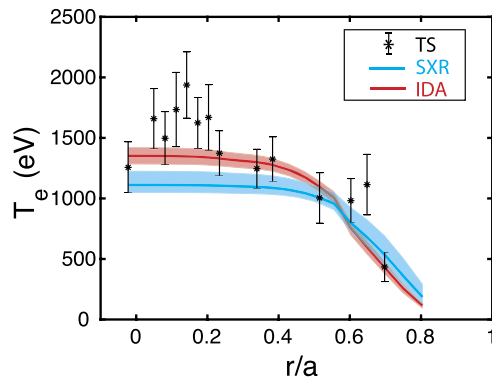


FIG. 2. Resulting IDA inference of the T_e profile (red curve) compared to the results from TS only (black stars) and SXR only (blue curve), all shown with 1σ error. Profiles inferred using SXR data and IDA both result in a 2D profile. Here a 1D slice consistent with TS has been plotted. Uncertainty in the profile inferred using IDA is smaller than profiles inferred using either TS or SXR alone. The discrepancy between SXR and TS is more fully discussed in the text.

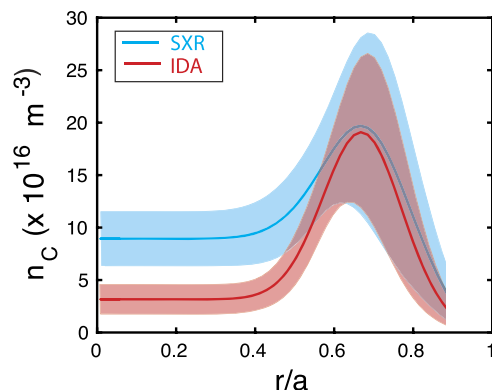


FIG. 3. Inference of a carbon density profile with 1σ error bands using SXR data only (blue curve) and IDA of SXR and TS data (red curve).

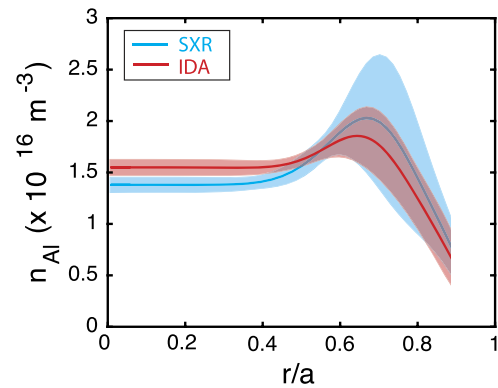


FIG. 4. Inference of an aluminum density profile with 1σ error bands using SXR data only (blue curve) and IDA of SXR and TS data (red curve).

along with the results from just the TS diagnostic (black stars) and using just SXR data (blue curve). The shaded region on the inferred SXR and IDA profiles represent the 1σ uncertainty, and the error bars represent the 1σ uncertainty for the TS points. The SXR and IDA inferences both result in a 2D profile for T_e , so the comparison here is a 1D slice that is consistent with TS.

Uncertainty in the profile inferred using IDA is smaller than profiles inferred using either TS or SXR alone and IDA finds a maximum in a different region in the parameter space. This can be understood through the correlation illustrated in Fig. 1(d) between carbon density and T_e . Without information from TS, marginalization over all possible carbon densities results in a probability distribution for T_e that is skewed toward lower T_e . Information from TS constrains the probability distribution to a different part of the distribution. While the likelihood functions in Fig. 2 are for illustrative purposes only, such correlations do exist between the impurity densities and T_e . Likewise, because SXR brightness data are line integrated, there is a similar correlation between the steepness of the edge [α from Eq. (4)] and the peak temperature [T_{e0} from Eq. (4)], which can also be constrained with information from TS. It should be noted that the TS results here are somewhat degraded in quality due to unavoidable damage to the collection optics. Nevertheless, such data still provide a useful constraint within the IDA framework because

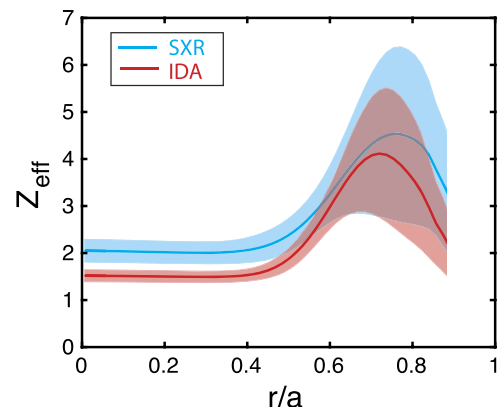


FIG. 5. Inference of Z_{eff} with 1σ error bands using only data from SXR data (blue curve) and IDA of SXR and TS data (red curve).

information on T_e is still present, albeit more uncertain in this case than when there is no damage. In particular, for this example, the localized nature of the TS diagnostic provides useful constraints both on the location of the maximum probability for temperature as well as constraining the profile shape, resulting in a slight difference in the edge temperature.

While IDA encourages awareness of all the information available, it also encourages examining the validity of assumptions and results. For example, this inference of the T_e profile is the best profile given all of the information, assuming that the profile shape is correct [i.e., Eq. (4) is a good description of the profile]. In particular, for this example, we have assumed that the temperature profile is axisymmetric with no fluctuations. It is entirely possible that the apparent fluctuation near $r/a = 0.2$ is real. While we do believe that the simple shape from the IDA inference of T_e is a more accurate description of the temperature profile in this plasma because of the large uncertainty in the TS data, this assumption can be explicitly tested by choosing a different form for the T_e profile by including such a feature in the profile. This is a subject of ongoing analysis and does represent a situation where calculation of the evidence is important in order to discriminate between the two profile descriptions.

As was indicated in the illustration using synthetic data in Fig. 1, the combination of TS and SXR brightness data can constrain the impurity density profiles. This IDA tool allows inferences of all known impurities, giving us detailed information not just on Z_{eff} but on the underlying impurity densities as well. Profiles for two impurities, carbon and aluminum, are shown in Figs. 3 and 4, respectively. These figures show the inference of the impurity profiles using just SXR data (blue curve) and the IDA inference (red curve). Again, the shaded region shows the 1σ uncertainty. Here, there is no comparison to TS because TS contains no information on impurity densities. The discrepancy in the core is due to the discrepancy in the T_e profiles as discussed above. The hollow shape of these profiles is consistent with the thermal screening effect and is expected for this plasma.

The inferred Z_{eff} profile based on the inferred impurity density profiles is shown in Fig. 5. This curve represents the most likely profile for Z_{eff} in this plasma given all of the information available. This is a significant extension of measurement capability on MST because as mentioned, attempts to measure Z_{eff} using single-diagnostic methods were unsuccessful. Z_{eff} on MST can only be obtained through application of IDA.

As with the T_e profile, the profiles in Figs. 3–5 represent the most likely profiles given all the information and assuming that the models are appropriate. Here, the Z_{eff} profile is calculated directly from the impurity density profiles, so there are no assumptions about Z_{eff} explicitly; however, we have made several simplifying assumptions regarding the impurities as described above. Such assumptions may lead to the bias of our interpretation in our results;³⁶ however, explicit awareness of these assumptions enables us to test such assumptions. There are strong physics reasons behind choosing the hollow shape in this example, but there may be situations in which different physical mechanisms dominate and the hollow profiles would not be a good description.

Another assumption of this analysis is that we have included all impurities in the model that are present in the plasma. However, there is often some doubt as to the completeness of using CHERS to measure impurity densities, as resources are typically not available to measure the concentration of every possible plasma impurity, calling into question whether the list of impurities explicitly included in the model is sufficient. We have tested this potential limitation in our model by explicitly allowing the presence of unknown test impurities. Specifically we allowed either argon, representing mid-Z impurities, or helium, representing low-Z impurities, to be present in the plasma.³⁹ It was found that argon may be present in trace amounts; however, the maximum possible density was sufficiently small that it had a minimal effect on the inference of Z_{eff} . Similarly, while helium may be present in larger amounts than argon, the charge of helium is so low that it also has minimal effect on Z_{eff} . This analysis gives us confidence that if there are other impurities in the plasma and their effect is negligible; thus, our model is suitable.

The benefits of IDA identified here will become more pronounced as we move to larger and more powerful fusion experiments. The severe limitations imposed by the operation of diagnostics in nuclear environments mean that data will be simultaneously very difficult to obtain and are very valuable. This means that maximum scientific values must be extracted from each set of diagnostic measurements, and IDA provides the means to do so.

SUPPLEMENTARY MATERIAL

See [supplementary material](#) for data used to generate Figs. 2–5 in this document, which is available online.

ACKNOWLEDGMENTS

This material is based upon work supported by the U.S. Department of Energy Office of Science, Office of Fusion Energy Sciences program under Award Nos. DE-FC02-05ER54814 and DE-SC0015474.

- ¹I. H. Hutchinson, “Electromagnetic emission by free electrons,” in *Principles of Plasma Diagnostics*, 2nd ed. (Cambridge University Press, 2002), p. 155.
- ²F. C. Jahoda, E. M. Little, W. E. Quinn, G. A. Sawyer, and T. F. Stratton, *Phys. Rev.* **119**, 843 (1960).
- ³T. P. Donaldson, *Plasma Phys.* **20**, 1279 (1978).
- ⁴R. Fischer, E. Wolfrum, J. Schweinzer, and ASDEX Upgrade Team, *Plasma Phys. Controlled Fusion* **50**, 085009 (2008).
- ⁵O. Ford, J. Svensson, A. Boboc, and D. C. McDonald, *Rev. Sci. Instrum.* **79**, 10F324 (2008).
- ⁶M. Krychowiak, M. Brix, D. Dodt, Y. Feng, R. König, O. Schmitz, J. Svensson, and R. Wolf, *Plasma Phys. Controlled Fusion* **53**, 035019 (2011).
- ⁷D. Li, J. Svensson, H. Thomsen, F. Medina, A. Werner, and R. Wolf, *Rev. Sci. Instrum.* **84**, 083506 (2013).
- ⁸A. Langenberg, J. Svensson, H. Thomsen, O. Marchuk, N. A. Pablant, R. Burhenn, and R. C. Wolf, *Fusion Sci. Technol.* **69**, 560 (2016).
- ⁹D. Sivia, *Data Analysis: A Bayesian Tutorial*, 2nd ed. (Oxford University Press, New York, 2002).
- ¹⁰U. von Toussaint, *Rev. Mod. Phys.* **83**, 943 (2011).
- ¹¹R. Fischer, A. Dinklage, and E. Pasch, *Plasma Phys. Controlled Fusion* **45**, 1095 (2003).
- ¹²J. Svensson, A. Dinklage, J. Geiger, A. Werner, and R. Fischer, *Rev. Sci. Instrum.* **75**, 4219 (2004).

- ¹³O. Ford, "Tokamak plasma analysis through Bayesian diagnostic modelling," Ph.D. thesis, University of London, Imperial College London, 2010.
- ¹⁴B. P. van Milligen, T. Estrada, E. Ascasíbar, D. Tafalla, D. López-Bruna, A. López Fraguas, J. A. Jiménez, I. García-Cortés, A. Dinklage, and R. Fischer, *Rev. Sci. Instrum.* **82**, 073503 (2011).
- ¹⁵B. van Milligen, M. Pedrosa, C. Hidalgo, B. Carreras, T. Estrada, J. Alonso, J. de Pablos, A. Melnikov, L. Krupnik, L. Eliseev, and S. Perfilov, *Nucl. Fusion* **51**, 113002 (2011).
- ¹⁶R. Fischer, C. J. Fuchs, B. Kurzan, W. Suttrop, and E. Wolfrum, *Fusion Sci. Technol.* **58**, 675 (2010).
- ¹⁷A. Burckhart, E. Wolfrum, R. Fischer, K. Lackner, and H. Zohm, *Plasma Phys. Controlled Fusion* **52**, 105010 (2010).
- ¹⁸M. Willensdorfer, E. Fable, E. Wolfrum, F. Aumayr, R. Fischer, F. Reimold, and F. Rytter, *J. Nucl. Mater.* **463**, 1091 (2015).
- ¹⁹E. Wolfrum, E. Viezzer, A. Burckhart, M. Dunne, P. Schneider, M. Willensdorfer, E. Fable, R. Fischer, D. Hatch, F. Jenko, B. Kurzan, P. Manz, and S. Rathgeber, *Nucl. Fusion* **55**, 053017 (2015).
- ²⁰R. Fischer, A. Bock, M. Dunne, J. C. Fuchs, L. Giannone, K. Lackner, P. J. McCarthy, E. Poli, R. Preuss, M. Rampp, M. Schubert, J. Stober, W. Suttrop, G. Tardini, M. Weiland, and ASDEX Upgrade Team, *Fusion Sci. Technol.* **69**, 526 (2016).
- ²¹J. Svensson, O. Ford, D. C. McDonald, A. Meakins, A. Werner, M. Brix, A. Boboc, M. Beurskens, and JET EFDA Contributors, *Contrib. Plasma Phys.* **51**, 152 (2011).
- ²²J. K. Anderson, P. L. Andrew, B. E. Chapman, D. Craig, and D. J. Den Hartog, *Rev. Sci. Instrum.* **74**, 2107 (2003).
- ²³D. J. Clayton, A. F. Almagri, D. R. Burke, C. B. Forest, J. A. Goetz, M. C. Kaufman, and R. O'Connell, *Rev. Sci. Instrum.* **81**, 10E308 (2010).
- ²⁴S. T. A. Kumar, D. J. Den Hartog, V. V. Mirnov, K. J. Caspary, R. M. Magee, D. L. Brower, B. E. Chapman, D. Craig, W. X. Ding, S. Eilerman, G. Fiksel, L. Lin, M. Nornberg, E. Parke, J. A. Reusch, and J. S. Sarff, *Phys. Plasmas* **19**, 056121 (2012).
- ²⁵S. T. A. Kumar, D. J. Den Hartog, B. E. Chapman, M. O'Mullane, M. Nornberg, D. Craig, S. Eilerman, G. Fiksel, E. Parke, and J. A. Reusch, *Plasma Phys. Controlled Fusion* **54**, 012002 (2012).
- ²⁶S. T. A. Kumar, D. J. Den Hartog, K. J. Caspary, R. M. Magee, V. V. Mirnov, B. E. Chapman, D. Craig, G. Fiksel, and J. S. Sarff, *Phys. Rev. Lett.* **108**, 125006 (2012).
- ²⁷T. Barbui, L. Carraro, D. J. Den Hartog, S. T. A. Kumar, and M. Nornberg, *Plasma Phys. Controlled Fusion* **56**, 075012 (2014).
- ²⁸J. A. Reusch, M. T. Borchardt, D. J. Den Hartog, A. F. Falkowski, D. J. Holly, R. O'Connell, and H. D. Stephens, *Rev. Sci. Instrum.* **79**, 10E733 (2008).
- ²⁹A. C. Selden, *Phys. Lett. A* **79**, 405 (1980).
- ³⁰H. D. Stephens, "Electron temperature structures associated with magnetic tearing modes in the Madison symmetric torus," Ph.D. thesis, University of Wisconsin-Madison, 2010.
- ³¹M. B. McGarry, P. Franz, D. J. Den Hartog, and J. A. Goetz, *Rev. Sci. Instrum.* **81**, 10E516 (2010).
- ³²L. M. Reusch, P. Franz, D. J. Den Hartog, J. A. Goetz, M. D. Nornberg, and P. VanMeter, *Fusion Sci. Technol.* **74**, 167 (2018).
- ³³L. M. Reusch, D. J. Den Hartog, P. Franz, J. A. Goetz, M. B. McGarry, and H. D. Stephens, *Rev. Sci. Instrum.* **87**, 11E332 (2016).
- ³⁴M. B. McGarry, P. Franz, D. J. Den Hartog, J. A. Goetz, and J. Johnson, *Rev. Sci. Instrum.* **85**, 096105 (2014).
- ³⁵F. Bonomo, A. Alfier, M. Gobbin, F. Auremma, P. Franz, L. Marrelli, R. Pasqualotto, G. Spizzo, and D. Terranova, *Nucl. Fusion* **49**, 045011 (2009).
- ³⁶L. M. Reusch, M. E. Galante, P. Franz, J. R. Johnson, M. B. McGarry, H. D. Stephens, and D. J. Den Hartog, *Rev. Sci. Instrum.* **85**, 11D844 (2014).
- ³⁷H. P. Summers, *The ADAS User Manual* (2004).
- ³⁸H. P. Summers, W. J. Dickson, M. G. O'Mullane, N. R. Badnell, A. D. Whiteford, D. H. Brooks, J. Lang, S. D. Loch, and D. C. Griffin, *Plasma Phys. Controlled Fusion* **48**, 263 (2006).
- ³⁹M. E. Galante, L. M. Reusch, D. J. Den Hartog, P. Franz, J. R. Johnson, M. B. McGarry, M. D. Nornberg, and H. D. Stephens, *Nucl. Fusion* **55**, 123016 (2015).
- ⁴⁰M. Nornberg, D. Den Hartog, and L. Reusch, *Fusion Sci. Technol.* **74**, 144 (2018).
- ⁴¹D. Foreman-Mackey, D. W. Hogg, D. Lang, and J. Goodman, *Publ. Astron. Soc. Pac.* **125**, 306 (2013).